

# Topological susceptibility and axion properties in the presence of a strong magnetic field within the three-flavor NJL model

J. P. Carlomagno<sup>1,2,\*</sup>, D. Gómez Dumm<sup>1,2</sup> and N. N. Scoccola<sup>2,3</sup>

<sup>1</sup>*Instituto de Física La Plata, CONICET—Departamento de Física, Facultad de Ciencias Exactas, Universidad Nacional de La Plata, C.C. 67, 1900 La Plata, Argentina*

<sup>2</sup>*CONICET, Rivadavia 1917, 1033 Buenos Aires, Argentina*

<sup>3</sup>*Physics Department, Comisión Nacional de Energía Atómica, Avenida del Libertador 8250, 1429 Buenos Aires, Argentina*



(Received 8 January 2025; accepted 17 March 2025; published 1 April 2025)

We analyze the topological susceptibility and the axion properties in the presence of an external uniform magnetic field, considering a three-flavor Nambu–Jona-Lasinio model that includes strong  $CP$  violation through a 't Hooft-like flavor mixing term. Both thermal and finite density effects are studied for magnetic fields up to  $1 \text{ GeV}^2$ , and the corresponding phase transitions are analyzed. To capture the inverse magnetic catalysis effect at finite temperatures and densities, a magnetic-field-dependent coupling constant is considered. Our analytical and numerical results are compared with those previously obtained from lattice QCD, chiral perturbation theory, and other effective models.

DOI: [10.1103/PhysRevD.111.074001](https://doi.org/10.1103/PhysRevD.111.074001)

## I. INTRODUCTION

As is well known, QCD contains gauge field configurations that carry topological charge [1]. These configurations interpolate between different vacua of the gluonic sector, giving rise to the so-called “ $\theta$  vacuum” [2]. At the level of the QCD Lagrangian, this nontrivial nature of the QCD vacuum implies the presence of a so-called  $\theta$  term of the form

$$\mathcal{L}_\theta = \theta_0 \frac{g^2}{32\pi^2} G_{\mu\nu} \tilde{G}^{\mu\nu}, \quad (1)$$

where  $g$  is the strong coupling constant, and  $G_{\mu\nu}$  and  $\tilde{G}_{\mu\nu}$  stand for the gluon field tensor and its dual. In fact, in the context of the full Standard Model, the coefficient  $\theta_0$  can be modified through a chiral rotation. Considering the weak interaction sector, by diagonalizing the Yukawa-generated quark mass matrix  $M_q$ , one has

$$\theta_0 \rightarrow \theta = \theta_0 + \arg \det M_q. \quad (2)$$

The parameter  $\theta$  (which can be taken to run from 0 to  $2\pi$ , due to the periodicity of the action) can be, in principle,

\*Contact author: [carlomagno@fisica.unlp.edu.ar](mailto:carlomagno@fisica.unlp.edu.ar)

Published by the American Physical Society under the terms of the [Creative Commons Attribution 4.0 International](https://creativecommons.org/licenses/by/4.0/) license. Further distribution of this work must maintain attribution to the author(s) and the published article's title, journal citation, and DOI. Funded by SCOAP<sup>3</sup>.

experimentally determined. Presently, measurements of the neutron electric dipole moment lead to the constraint  $|\theta| \lesssim 10^{-11}$ . Since a nonzero value of  $\theta$  would imply the existence of  $CP$  violation in the strong interaction sector, the measurement of such an unexpectedly low upper bound for the value of  $|\theta|$  is known as the “strong  $CP$  problem.”

As proposed almost 50 years ago by Peccei and Quinn, a possible solution for this puzzle can be achieved by invoking the existence of an additional global  $U(1)$  chiral symmetry [3,4]. The spontaneous breakdown of this symmetry leads to the presence of an associated Goldstone boson, the axion, which implies an extra anomalous contribution to the Lagrangian. Thus, the resulting effective potential gets minimized for a nonzero vacuum expectation value of the axion field, leading finally to a cancellation of the  $\theta$  term and solving the strong  $CP$  problem. In practice, the above-described mechanism can be basically implemented by promoting the parameter  $\theta$  to a dynamical field  $a$ , normalized by a dimensionful “decay constant”  $f_a$ . The effective potential will be given by a periodic function of  $a/f_a$ , becoming minimized for  $\langle a \rangle = 0$ .

After the original introduction of the axion as a possible solution for the strong  $CP$  problem, its relevance has also been discussed in other contexts (for a recent review, see, e.g., Ref. [5]). For example, since axions are expected to be very light as well as weakly interacting particles (present constraints on their properties can be found in Sec. 90 of Ref. [6]), they have been proposed as candidates for cold dark matter. In this sense, the temperature dependence of the axion mass would play an important role in the estimation of its cosmic abundance [7–9]. Axions might also

play a key role in astrophysics, in particular for the anomalous cooling of neutron stars (see, e.g., Refs. [10,11]). In this framework, the influence of nonzero density and background magnetic fields on the axion properties deserves particular interest.

The strength of the topological charge fluctuations in the QCD vacuum is quantified by the topological susceptibility  $\chi_t$ , which is defined as a second derivative of the QCD partition function with respect to  $\theta$  and is shown to be proportional to the axion mass  $m_a$ . Different approaches to nonperturbative QCD have been used to determine this quantity and other axion properties. In the context of lattice QCD (LQCD), results for  $\chi_t$  at zero and finite temperature can be found in Refs. [12–14]. Within the framework of effective models of the Nambu–Jona-Lasinio (NJL) type, estimates of the topological susceptibility, including its temperature dependence, have been obtained in Refs. [15–17]. More recently, the effect of the chiral phase transition on the axion mass and self-coupling within this scheme was studied in Ref. [18]. Extension of those analyses to finite chemical potential have been considered in Refs. [19–23].

In addition, considerable attention has been paid to the modifications of  $\chi_t$  and axion properties induced by the presence of strong magnetic fields. Besides its importance within the above-mentioned astrophysical context, it has been realized that the effect of magnetic fields on the topological structure of the QCD vacuum can be significant for the study of heavy ion collisions. In fact, the existence of a chirality imbalance induced by topology, in the presence of strong magnetic fields produced in a noncentral heavy ion collision, can lead to the so-called chiral magnetic effect, according to which positive and negative charges get separated along the magnetic field direction [24,25]. As discussed in Ref. [26], it is important to take into account the effects of both the temperature and the magnetic field on QCD vacuum fluctuations. These effects have been analyzed using chiral perturbation theory (ChPT) [27–29], which should be adequate for relatively low values of the magnetic field. In addition, results have been obtained using two-flavor versions of the local [30] and nonlocal NJL model [31]. One of the aims of the present work is to extend those studies by considering a three-flavor version of the local NJL model. It is worth pointing out that in the SU(3) chiral NJL model, the coupling that controls the flavor mixing effects related to the  $U(1)_A$  anomaly can be better determined, taking into account the phenomenological values of meson masses. Moreover, three-flavor models allow for a more consistent comparison with very recent results obtained using LQCD simulations with 2 + 1 flavors [32]. Another important purpose of our work is to complement previous studies by analyzing nonzero density effects, which, as already mentioned, might become relevant when axions are considered in astrophysical contexts.

This article is organized as follows. Following Ref. [33], in Sec. II A we review the general formalism corresponding to a three-flavor NJL model at finite temperature and chemical potential in the presence of a constant magnetic field, including the mentioned  $\theta$  field. Then, in Sec. II B, we derive the expressions needed to obtain the quantities of interest related to the topological susceptibility and the axion properties. Numerical results for these quantities are discussed in Sec. III. Finally, in Sec. IV, we summarize our results and present our main conclusions.

## II. THEORETICAL FORMALISM

### A. Effective NJL Lagrangian and mean field equations at zero temperature

We consider a three-flavor NJL Lagrangian that includes scalar and pseudoscalar chiral quark couplings as well as a 't Hooft six-fermion interaction term, in the presence of an external electromagnetic field  $A_\mu$ . Moreover, we take into account the coupling to a field  $\theta(x) = a(x)/f_a$  of the form given by Eq. (1). This can be effectively done through the 't Hooft term [which accounts for the chiral  $U(1)_A$  anomaly] by performing a chiral rotation of quark fields by an angle  $\theta$ . In this way, the effective Euclidean action is given by [33,34]

$$S_E = \int d^4x \left\{ \bar{\psi}(-i\not{D} + \hat{m})\psi - G \sum_{a=0}^8 [(\bar{\psi}\lambda_a\psi)^2 + (\bar{\psi}i\gamma_5\lambda_a\psi)^2] + K(e^{i\theta}d_+ + e^{-i\theta}d_-) \right\}, \quad (3)$$

where  $G$  and  $K$  are coupling constants,  $\psi = (\psi_u, \psi_d, \psi_s)^T$  stands for a quark three-flavor vector,  $\hat{m} = \text{diag}(m_u, m_d, m_s)$  is the corresponding current quark mass matrix, and  $d_\pm = \det[\bar{\psi}(1 \pm \gamma_5)\psi]$ . In addition,  $\lambda_a$  denote the Gell-Mann matrices, with  $\lambda_0 = \sqrt{2/3}I$ , where  $I$  is the unit matrix in the three-flavor space. The coupling of quarks to the electromagnetic field is implemented through the covariant derivative  $D_\mu = \partial_\mu - i\hat{Q}A_\mu$ , where  $\hat{Q} = \text{diag}(Q_u, Q_d, Q_s)$  represents the quark electric charge matrix, i.e.,  $Q_u/2 = -Q_d = -Q_s = e/3$ , with  $e$  being the proton electric charge. In the present work, we consider a static and constant magnetic field in the 3-direction.

We proceed by bosonizing the action in terms of scalar  $\sigma_a(x)$  and pseudoscalar  $\pi_a(x)$  fields, also introducing corresponding auxiliary  $s_a(x)$  and  $p_a(x)$  fields. Following a standard procedure, we start from the partition function

$$Z = \int D\bar{\psi}D\psi e^{-S_E}. \quad (4)$$

By introducing functional delta functions, the scalar ( $\bar{\psi}\lambda_a\psi$ ) and pseudoscalar ( $\bar{\psi}i\gamma_5\lambda_a\psi$ ) currents in  $S_E$  can be replaced by  $s_a(x)$  and  $p_a(x)$ , and one can perform the functional integration on the fermionic fields  $\psi$  and  $\bar{\psi}$ . Then, to carry out the integration over the auxiliary fields, we use the stationary phase approximation (SPA), keeping the functions  $\tilde{s}_a(x)$  and  $\tilde{p}_a(x)$  that minimize the integrand of the partition function. This yields a set of coupled equations among the bosonic fields, from which one can take  $\tilde{s}_a(x)$  and  $\tilde{p}_a(x)$  to be implicit functions of  $\sigma_a(x)$  and  $\pi_a(x)$ . Finally, we consider the mean field (MF) approximation, expanding the bosonized action in powers of field fluctuations around the corresponding translationally invariant mean field values  $\bar{\sigma}_a$  and  $\bar{\pi}_a$ . Thus, we write  $\sigma_a(x) = \bar{\sigma}_a + \delta\sigma_a(x)$  and  $\pi_a(x) = \bar{\pi}_a + \delta\pi_a(x)$ , where, due to charge conservation, only  $\bar{\sigma}_a$  and  $\bar{\pi}_a$  with  $a = 0, 3$ , and  $8$  can be nonzero. For convenience, we introduce the notations  $\bar{\sigma} = \text{diag}(\bar{\sigma}_u, \bar{\sigma}_d, \bar{\sigma}_s) = \lambda_0\bar{\sigma}_0 + \lambda_3\bar{\sigma}_3 + \lambda_8\bar{\sigma}_8$  and  $\bar{\pi} = \text{diag}(\bar{\pi}_u, \bar{\pi}_d, \bar{\pi}_s) = \lambda_0\bar{\pi}_0 + \lambda_3\bar{\pi}_3 + \lambda_8\bar{\pi}_8$ .

At the mean field level, the Euclidean action per unit volume reads

$$\begin{aligned} \frac{\tilde{S}_E^{\text{bos}}}{V^{(4)}} = & -\frac{N_c}{V^{(4)}} \sum_f \int d^4x d^4x' \text{tr}_D \ln (\mathcal{S}_{x,x'}^f)^{-1} \\ & -\frac{1}{2} \sum_f [\bar{\sigma}_f \tilde{s}_f + \bar{\pi}_f \tilde{p}_f + G(\tilde{s}_f^2 + \tilde{p}_f^2)] \\ & + \frac{K}{4} [\cos \theta (\tilde{s}_u \tilde{s}_d \tilde{s}_s - \tilde{s}_u \tilde{p}_d \tilde{p}_s - \tilde{p}_u \tilde{s}_d \tilde{p}_s - \tilde{p}_u \tilde{p}_d \tilde{s}_s) \\ & - \sin \theta (\tilde{p}_u \tilde{p}_d \tilde{p}_s - \tilde{p}_u \tilde{s}_d \tilde{s}_s - \tilde{s}_u \tilde{p}_d \tilde{s}_s - \tilde{s}_u \tilde{s}_d \tilde{p}_s)], \end{aligned} \quad (5)$$

where  $\text{tr}_D$  stands for trace in Dirac space, while

$$(\mathcal{S}_{x,x'}^f)^{-1} = \delta(x-x')[-i(\not{\partial} - iQ_f \not{A}) + M_{sf} + i\gamma_5 M_{pf}] \quad (6)$$

is the inverse mean field quark propagator for each flavor. Here, we have used the definitions  $M_{sf} = m_f + \bar{\sigma}_f$  and  $M_{pf} = \bar{\pi}_f$ . Moreover, in Eq. (5),  $\tilde{s}_f$  are the values of the auxiliary fields at the mean field level within the SPA approximation, i.e.,  $\tilde{s}_f = \tilde{s}_f(\bar{\sigma}_a)$ . They satisfy the conditions

$$\bar{\sigma}_i + 2G\tilde{s}_i - \frac{K}{4} \sum_{jk} |\epsilon_{ijk}| [(\tilde{s}_j \tilde{s}_k - \tilde{p}_j \tilde{p}_k) \cos \theta + 2\tilde{s}_j \tilde{p}_k \sin \theta] = 0, \quad (7)$$

$$\bar{\pi}_i + 2G\tilde{p}_i - \frac{K}{4} \sum_{jk} |\epsilon_{ijk}| [(\tilde{s}_j \tilde{s}_k - \tilde{p}_j \tilde{p}_k) \sin \theta - 2\tilde{s}_j \tilde{p}_k \cos \theta] = 0, \quad (8)$$

where the values 1, 2, and 3 for indices  $i, j$ , and  $k$  are equivalent to labels  $f = u, d$ , and  $s$ , and  $|\epsilon_{ijk}|$  is the

absolute value of the Levi-Civita tensor. From the conditions  $\delta\tilde{S}_E^{\text{bos}}/\delta\bar{\sigma}_f = 0$  and  $\delta\tilde{S}_E^{\text{bos}}/\delta\bar{\pi}_f = 0$ , one can now get the “gap equations”

$$\bar{s}_f = 2\langle \bar{q}_f q_f \rangle, \quad \bar{p}_f = 2\langle \bar{q}_f i\gamma_5 q_f \rangle, \quad (9)$$

where the quark-antiquark condensates are given by

$$\begin{aligned} \langle \bar{q}_f q_f \rangle &= -\frac{N_c}{V^{(4)}} \int d^4x \text{tr}_D [\mathcal{S}_{x,x}^f], \\ \langle \bar{q}_f i\gamma_5 q_f \rangle &= -\frac{N_c}{V^{(4)}} \int d^4x \text{tr}_D [i\gamma_5 \mathcal{S}_{x,x}^f]. \end{aligned} \quad (10)$$

As is well known, the quark propagator can be written in different ways [35,36]. For convenience, we use an expression given by a product of a phase factor and a translational invariant function, namely,

$$\mathcal{S}_{x,x'}^f = e^{i\Phi_f(x,x')} \int \frac{d^4p}{(2\pi)^4} e^{ip(x-x')} \tilde{\mathcal{S}}_p^f. \quad (11)$$

Here,  $\Phi_f(x, x')$  is the so-called Schwinger phase, which depends on the gauge chosen to specify the  $\mathcal{A}_\mu$  field, while  $\tilde{\mathcal{S}}_p^f$  is a gauge invariant quantity. The latter can be expressed in the Landau level form

$$\begin{aligned} \tilde{\mathcal{S}}_p^f &= 2e^{-\vec{p}_\perp^2/B_f} \sum_{k=0}^{\infty} \frac{(-1)^k}{M_{sf}^2 + M_{pf}^2 + p_\parallel^2 + 2kB_f} \\ &\times \left\{ (M_{sf} - i\gamma_5 M_{pf} - p_\parallel \cdot \gamma_\parallel) \right. \\ &\times \left[ \Gamma_f^+ L_k \left( \frac{2\vec{p}_\perp^2}{B_f} \right) - \Gamma_f^- L_{k-1} \left( \frac{2\vec{p}_\perp^2}{B_f} \right) \right] \\ &\left. + 2\vec{p}_\perp \cdot \vec{\gamma}_\perp L_{k-1} \left( \frac{2\vec{p}_\perp^2}{B_f} \right) \right\}, \end{aligned} \quad (12)$$

where  $L_k^\alpha(x)$  are generalized Laguerre polynomials, with the convention  $L_{-1}^\alpha(x) = 0$ . We have also introduced the definitions  $s_f = \text{sign}(Q_f B)$  and  $B_f = |Q_f B|$ , together with  $\Gamma_f^\pm = (1 \pm is_f \gamma_1 \gamma_2)/2$ . “Perpendicular” and “parallel” gamma matrices have been collected into vectors  $\gamma_\perp = (\gamma_1, \gamma_2)$  and  $\gamma_\parallel = (\gamma_3, \gamma_4)$ , and, in the same way, we have defined vectors  $p_\perp = (p_1, p_2)$  and  $p_\parallel = (p_3, p_4)$ . Note that in our convention,  $\{\gamma_\mu, \gamma_\nu\} = -2\delta_{\mu\nu}$ .

Since the propagators in Eq. (10) are evaluated at  $x = x'$ , Schwinger phases vanish and the condensates turn out to be gauge-independent quantities. As usual, it is seen that the resulting expressions for  $\bar{s}_f$  and  $\bar{p}_f$  are divergent and have to be properly regularized. We use here the magnetic-field-independent regularization (MFIR) scheme [37–44], in which one subtracts from the unregulated integral the  $B \rightarrow 0$  limit and then adds it in a regulated form. In this way, we obtain

$$\bar{s}_f = -2N_c M_{sf} I_{1f}^B, \quad \bar{p}_f = -2N_c M_{pf} I_{1f}^B, \quad (13)$$

where

$$I_{1f}^B = I_{1f}^0 + I_{1f}^{\text{mag}}. \quad (14)$$

For the quantity  $I_{1f}^0$ , we use here a 3D cutoff regularization. Thus, we have

$$I_{1f}^0 = \frac{1}{2\pi^2} \left[ \Lambda \sqrt{\bar{M}_f^2 + \Lambda^2} + \bar{M}_f^2 \ln \left( \frac{\bar{M}_f}{\Lambda + \sqrt{\bar{M}_f^2 + \Lambda^2}} \right) \right], \quad (15)$$

where  $\bar{M}_f = \sqrt{M_{sf}^2 + M_{pf}^2}$ . On the other hand, the “magnetic piece”  $I_{1f}^{\text{mag}}$  is found to be given by

$$I_{1f}^{\text{mag}} = \frac{B_f}{2\pi^2} \left[ \ln \Gamma(x_f) - \left( x_f - \frac{1}{2} \right) \ln x_f + x_f - \frac{\ln 2\pi}{2} \right], \quad (16)$$

where  $x_f = \bar{M}_f^2/(2B_f)$  and  $\Gamma(x)$  is the usual Gamma function.

The associated Euclidean regularized action per unit volume is given by

$$\begin{aligned} \frac{\bar{S}_E^{\text{bos}}}{V^{(4)}} &= \sum_f \omega_f^B - \frac{1}{2} \sum_i [\bar{\sigma}_i \bar{s}_i + \bar{\pi}_i \bar{p}_i + G(\bar{s}_i^2 + \bar{p}_i^2)] \\ &+ \frac{K}{24} \sum_{ijk} |\epsilon_{ijk}| [\cos \theta(\bar{s}_i \bar{s}_j \bar{s}_k - 3\bar{s}_i \bar{p}_j \bar{p}_k) \\ &- \sin \theta(\bar{p}_i \bar{p}_j \bar{p}_k - 3\bar{p}_i \bar{s}_j \bar{s}_k)], \end{aligned} \quad (17)$$

where

$$\omega_f^B = \omega_f^0 + \omega_f^{\text{mag}}, \quad (18)$$

with

$$\begin{aligned} \omega_f^0 &= -\frac{N_c}{8\pi^2} \left[ \Lambda \sqrt{\bar{M}_f^2 + \Lambda^2} (\bar{M}_f^2 + 2\Lambda^2) \right. \\ &\left. + \bar{M}_f^4 \ln \left( \frac{\bar{M}_f}{\Lambda + \sqrt{\bar{M}_f^2 + \Lambda^2}} \right) \right], \end{aligned} \quad (19)$$

$$\omega_f^{\text{mag}} = -\frac{N_c B_f^2}{2\pi^2} \left[ \zeta'(-1, x_f) - \frac{x_f^2 - x_f}{2} \ln x_f + \frac{x_f^2}{4} \right]. \quad (20)$$

Here,  $\zeta'(-1, x_f)$  stands for the derivative of the Hurwitz zeta function.

Let us now consider the case of a system in equilibrium at a finite temperature  $T$  and quark chemical potential  $\mu$ . We follow here a similar analysis as the one carried out in

Ref. [33]. The expressions for the mean field values  $\bar{s}_f$  and  $\bar{p}_f$  can be written as in Eq. (13), replacing the function  $I_{1f}^B$  with

$$I_{1f}^{B,T,\mu} = I_{1f}^B + I_{1f}^{\text{mag},T,\mu}, \quad (21)$$

where

$$\begin{aligned} I_{1f}^{\text{mag},T,\mu} &= \frac{B_f}{4\pi^2} \sum_{k=0}^{\infty} \alpha_k \int_{-\infty}^{\infty} dp \frac{1}{E_{kpf}} \\ &\times \sum_{s=\pm} \frac{1}{1 + \exp[(E_{kpf} + s\mu)/T]}, \end{aligned} \quad (22)$$

with  $\alpha_k = 2 - \delta_{k0}$ ,  $E_{kpf} = \sqrt{p^2 + 2kB_f + \bar{M}_f^2}$ .

In the same way, the associated regularized thermodynamic potential  $\Omega$  can be expressed as in Eq. (17), replacing  $\omega_f^B$  with  $\omega_f^{B,T,\mu}$ , where

$$\omega_f^{B,T,\mu} = \omega_f^B + \omega_f^{\text{mag},T,\mu}. \quad (23)$$

The  $T = 0$ ,  $\mu = 0$  piece  $\omega_f^B$  is given by Eqs. (18)–(20), while the finite  $T$ ,  $\mu$  piece reads

$$\begin{aligned} \omega_f^{\text{mag},T,\mu} &= -\frac{N_c T}{4\pi^2} \sum_f B_f \sum_{k=0}^{\infty} \alpha_k \int_{-\infty}^{\infty} dp \\ &\times \sum_{s=\pm} \ln \{ 1 + \exp[-(E_{kpf} + s\mu)/T] \}. \end{aligned} \quad (24)$$

Notice that the mean field thermodynamical potential is written in terms of the functions  $\omega_f^{B,T,\mu}$  and the mean field values  $\bar{s}_f$  and  $\bar{p}_f$ , which are gauge invariant quantities.

## B. Mean field topological susceptibility, axion mass, and axion self-coupling

As stated, the topological susceptibility  $\chi_t$  is useful to analyze how the manifestations of the chiral anomaly are affected by the temperature and the external magnetic field. This quantity is given by

$$\chi_t = \int d^4x \langle 0 | T Q(x) Q(0) | 0 \rangle, \quad (25)$$

where  $Q(x)$  is the topological charge

$$Q(x) = \frac{g^2}{32\pi^2} G_{\mu\nu}(x) \tilde{G}^{\mu\nu}(x). \quad (26)$$

In the framework of the above-introduced effective NJL model,  $\chi_t$  can be simply calculated by taking the second derivative of the thermodynamic potential with respect to  $\theta$ ,

$$\chi_t = \left. \frac{d^2 \Omega}{d\theta^2} \right|_{\theta=0}. \quad (27)$$

The evaluation of the first derivative of  $\Omega$  with respect to  $\theta$  can be obtained by taking into account the SPA equations

$$\frac{\partial \Omega}{\partial \bar{s}_f} = \frac{\partial \Omega}{\partial \bar{p}_f} = 0, \quad (28)$$

together with the MF conditions

$$\frac{\partial \Omega}{\partial \bar{\sigma}_f} = \frac{\partial \Omega}{\partial \bar{\pi}_f} = 0. \quad (29)$$

Following the steps sketched in the Appendix, from these equations one gets

$$\frac{d\Omega}{d\theta} = -\frac{1}{2} m_f \bar{p}_f, \quad (30)$$

where  $f$  can be either  $u$ ,  $d$ , or  $s$ .

Notice that if any of the current quark masses (e.g.,  $m_u$ ) are taken to be equal to zero, one immediately obtains  $d\Omega/d\theta = 0$ , i.e., the Lagrangian in Eq. (3) becomes independent of  $\theta$ . This is due to the existence of an additional U(1) global symmetry. In this limit, the value of  $\theta$  becomes unobservable, and, as is well known, the strong  $CP$  problem vanishes.

From Eqs. (13), (30), and (A1), it is seen that, as required by the Peccei-Quinn mechanism, the minimization condition  $d\Omega/d\theta = 0$  leads to the mean field values  $\bar{\pi}_f = 0$  and  $\bar{\theta} = 0$ . On the other hand, at the mean field level, the second derivative of the action with respect to  $a = f_a \theta$  is nothing but the axion mass squared. Thus, the topological susceptibility and the axion mass are simply related by

$$f_a^2 m_a^2 = \left. \frac{d^2 \Omega}{d\theta^2} \right|_{\theta=\bar{\theta}=0} = \chi_t. \quad (31)$$

As discussed in the Appendix, after some calculation we obtain

$$\chi_t = -\frac{1}{2} \left[ \frac{2}{K \bar{s}_u \bar{s}_d \bar{s}_s} + \sum_k \frac{1}{m_k \bar{s}_k} \right]^{-1}. \quad (32)$$

We recall that  $\bar{s}_f$  is equal to twice the scalar condensate  $\langle \bar{q}_f q_f \rangle$ .

The above expression can be compared to previous results obtained in the approximate chiral limit, where current masses are taken to be relatively small. At the lowest order in  $m_f^{-1}$ , one has

$$\chi_t \simeq -\frac{1}{2} \left( \sum_k \frac{1}{m_k \bar{s}_k} \right)^{-1}. \quad (33)$$

Moreover, assuming  $\bar{s}_u \simeq \bar{s}_d \simeq \bar{s}_s$ , one can approximate

$$\chi_t \simeq -\frac{\frac{1}{2} \sum_k \frac{\bar{s}_k}{m_k}}{\left( \sum_k \frac{1}{m_k} \right)^2} + \mathcal{O}(\Delta_{su}^2, \Delta_{du} \Delta_{su}, \Delta_{du}^2), \quad (34)$$

where  $\Delta_{fu} = (\bar{s}_f - \bar{s}_u)/\bar{s}_u$ . This is in agreement with the expressions found in Refs. [29,45,46] in the contexts of ChPT and a linear sigma model, respectively. In the limit  $\bar{s}_u = \bar{s}_d = \bar{s}_s$ , the above expressions for  $\chi_t$  reduce to the lowest-order ChPT Leutwyler-Smilga relation [47]

$$\chi_t \simeq -\frac{\bar{s}_f}{2} \left( \sum_k \frac{1}{m_k} \right)^{-1}. \quad (35)$$

Finally, it is also interesting to study the axion self-coupling arising from the  $\theta$ -dependent effective potential. It is usual to focus on the  $\theta^4$  [i.e.,  $(a/f_a)^4$ ] term in the effective action, defining the coupling parameter  $\lambda_a$  as

$$\lambda_a = \left. \frac{1}{f_a^4} \frac{d^4 \Omega}{d\theta^4} \right|_{\theta=0}. \quad (36)$$

### III. RESULTS

#### A. Model parameters

Before presenting the numerical results for the topological susceptibility, we introduce the parametrization that has been chosen for the above-discussed three-flavor version of the NJL model. Following Refs. [48,49], we adopt the parameter set  $m_u = m_d = 5.5$  MeV,  $m_s = 140.7$  MeV,  $\Lambda = 602.3$  MeV,  $G\Lambda^2 = 1.835$ , and  $K\Lambda^5 = 12.36$ . This set has been determined in such a way that for  $B = T = 0$ , one obtains meson masses  $m_\pi = 135$  MeV,  $m_K = 497.7$  MeV, and  $m_{\eta'} = 957.8$  MeV, together with a pion decay constant  $f_\pi = 92.4$  MeV.

It is well known that local NJL-like models fail to reproduce the inverse magnetic catalysis (IMC) effect at finite temperature. To address this issue, the possibility of allowing the coupling constant  $G$  to depend on the magnetic field has been considered [50–52]. Taking into account the analysis carried out in Ref. [50], we consider a functional form

$$G(B) = G \left[ \frac{1 + a(eB/\Lambda_{\text{QCD}}^2)^2 + b(eB/\Lambda_{\text{QCD}}^2)^3}{1 + c(eB/\Lambda_{\text{QCD}}^2)^2 + d(eB/\Lambda_{\text{QCD}}^2)^4} \right], \quad (37)$$

where the parameters  $a$ ,  $b$ ,  $c$ , and  $d$  are determined by fitting the  $B$  dependence of the pseudocritical chiral transition temperatures to those obtained through LQCD calculations [53]. The values of the parameters are [50]  $a = 0.0108805$ ,  $b = -1.0133 \times 10^{-4}$ ,  $c = 0.02228$ , and  $d = 1.84558 \times 10^{-4}$ , with  $\Lambda_{\text{QCD}} = 300$  MeV. The effect

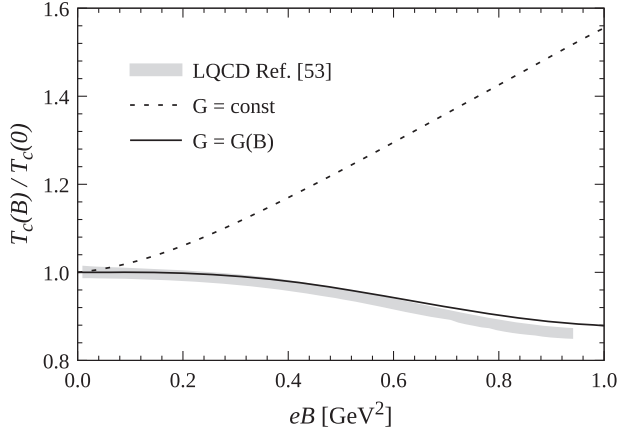


FIG. 1. Normalized values of the pseudocritical chiral restoration temperatures as functions of the magnetic field, for constant and  $B$ -dependent  $G$  [50]. Lattice QCD results from Ref. [53] are included for comparison.

on the pseudocritical chiral restoration temperatures  $T_c$  (at zero baryon chemical potential) is shown in Fig. 1, where we plot  $T_c$ —normalized to  $T_c(B=0)$ —as a function of the magnetic field, considering the case of a constant coupling  $G$  and the case in which one has a  $B$ -dependent coupling  $G(B)$ , as in Eq. (37) [50]. For comparison, the  $B$  dependence of the normalized pseudocritical temperatures obtained from lattice QCD calculations is also shown (gray band in the figure) [53]. The normalization temperature in our model is found to be  $T_c(B=0) = 173$  MeV, somewhat larger than the critical value obtained from LQCD calculations,  $T_c(B=0) = 156$  MeV [54].

### B. Zero chemical potential

Let us start by quoting our numerical results for both zero quark chemical potential and zero temperature. In Fig. 2, we show the values of the topological susceptibility  $\chi_t$  (upper panel) and the axion self-coupling parameter  $\lambda_a$  (lower panel) as functions of the magnetic field, normalized by the corresponding values at  $B=0$ , namely,  $\chi_t(B=0) = 78$  MeV and  $\lambda_a(B=0) = 0.85 \times 10^{-5} \text{ GeV}^4/f_a^4$ .

Black dashed and solid lines in Fig. 2 correspond to  $G = \text{constant}$  and  $G = G(B)$ , respectively. It can be seen that in both cases,  $\chi_t$  and  $\lambda_a$  show an enhancement with the magnetic field. Within errors, our results for the topological susceptibility are shown to be in agreement with those obtained from LQCD calculations (blue squares) [32] for a temperature  $T \simeq 110$  MeV (which is well below the critical temperature and, therefore, the value of  $\chi_t$  should be rather close to the one at  $T=0$ ). In addition, we include for comparison the curves for  $\chi_t$  corresponding to a two-flavor NJL model, taken from Ref. [30], both for constant and  $B$ -dependent couplings (red dashed and solid lines, respectively). The above-mentioned value for  $\chi_t$  at  $B=0$  obtained within our model can be compared with the results obtained from ChPT [55] and LQCD [12] analyses,

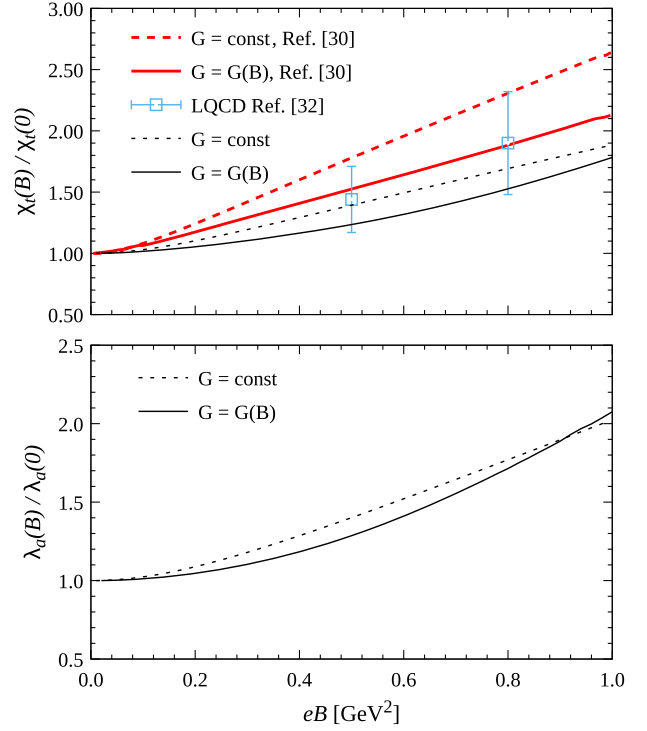


FIG. 2. Normalized values of  $\chi_t$  and  $\lambda_a$  as functions of  $eB$  for  $\mu = T = 0$ . The cases  $G = \text{const} \times \tan t$  and  $G = G(B)$  are considered. Results from a two-flavor NJL model [30] and LQCD [32] are shown for comparison.

which lead to  $\chi_t(B=0) \simeq 75.5$  MeV. In the case of the axion self-coupling, from ChPT the estimation  $\lambda_a \simeq 1.12 \times 10^{-5} \text{ GeV}^4/f_a^4$  is obtained [56].

The behavior of the above quantities for nonzero temperatures is shown in Fig. 3, where we show the numerical results for  $\chi_t^{1/4}$  and  $\lambda_a f_a^4$  as functions of  $T/T_c(B)$  for three representative values of the magnetic field. According to Eq. (22), here, a sum over Landau levels is required. For low temperatures, we find that our numerical calculations for  $\bar{s}_f$  and  $\bar{p}_f$  get convergence by taking a relatively low number of levels, even for low values of the magnetic field (about 30 levels guarantee an accuracy better than 0.01% for  $eB \gtrsim 0.03 \text{ GeV}^2$ ). Though the required number of levels gets somewhat increased for larger temperatures, it is found to be numerically manageable for the full considered temperature range. The pseudocritical chiral transition temperatures  $T_c(B)$  have been defined, taking the maximum values of the slopes  $d\bar{s}_l/dT$ , where  $\bar{s}_l = (\bar{s}_u + \bar{s}_d)/2$ , for each value of the magnetic field. Left and right panels correspond to the results for constant and  $B$ -dependent couplings, respectively. As expected, one finds a sudden drop of both  $\chi_t^{1/4}$  and  $\lambda_a$  at  $T = T_c$ , signaling the restoration of chiral symmetry in the light quark sector. Notice that the curves for  $\lambda_a$  tend to show a peak located at  $T = T_c$ , and this feature has also been observed in the context of NJL-like models in Refs. [20,21,30].

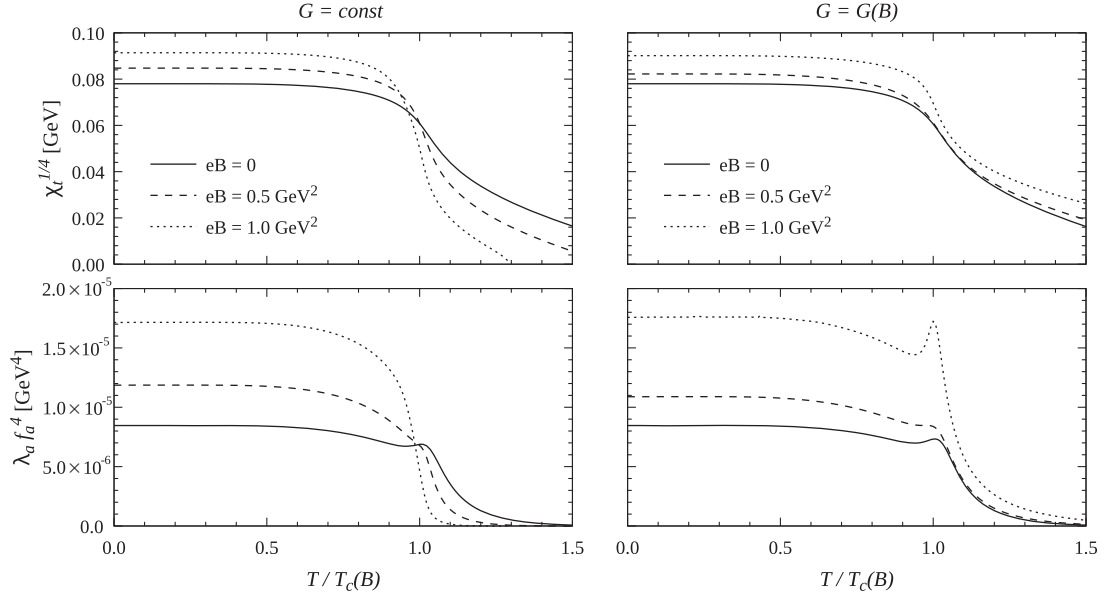


FIG. 3. Values of  $\chi_t^{1/4}$  and  $\lambda_a f_a^4$  as functions of  $T/T_c(B)$  for some representative values of the magnetic field.

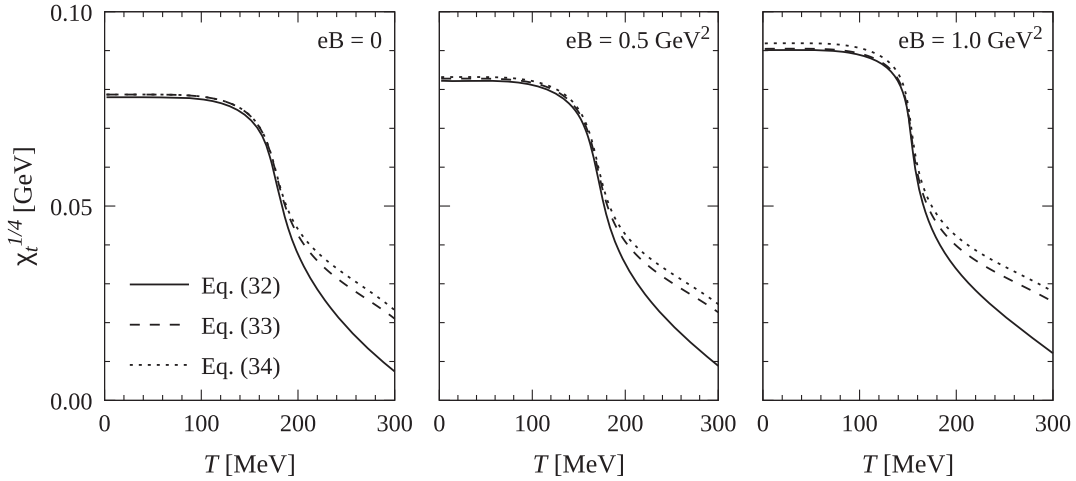


FIG. 4. Values of  $\chi_t^{1/4}$ , as calculated within our model, Eq. (32), compared with the results arising from the approximate expressions in Eqs. (33) and (34), for three different values of the magnetic field. The curves correspond to the case  $G = G(B)$ .

In Fig. 4, we compare the results for  $\chi_t^{1/4}$  obtained within our model, Eq. (32) (solid lines), with those arising from the approximate expressions in Eqs. (33) and (34) (dashed and dotted lines, respectively). The curves correspond to the case  $G = G(B)$ , for  $eB = 0, 0.5 \text{ GeV}^2$ , and  $1 \text{ GeV}^2$ . It can be seen that up to  $T \simeq T_c$ , all expressions are approximately equivalent for the considered values of the magnetic field. Beyond the chiral restoration transition, the curves corresponding to the approximate expressions in Eqs. (33) and (34) show some deviation with respect to the full result in Eq. (32). This difference is mainly due to the fact that the first term into the brackets, on the right-hand side of Eq. (32), becomes non-negligible in this region.

Our numerical results for the temperature dependence of  $\chi_t$  can also be compared with those recently obtained from LQCD calculations, see Ref. [32]. To perform the comparison, we consider the normalized quantity  $R_\chi \equiv \chi_t(B, T)/\chi_t(0, T)$  introduced in that work. In Fig. 5, we show our results (black curves) together with those quoted in Ref. [32] (shaded bands) for  $eB = 0.5$  and  $0.8 \text{ GeV}^2$ . We include in the figure just the curves that correspond to the case of the  $B$ -dependent coupling  $G(B)$ , which, as stated, is the one consistent with LQCD results for IMC. Once again, it is seen that the predictions of the NJL model show qualitative agreement with LQCD calculations.

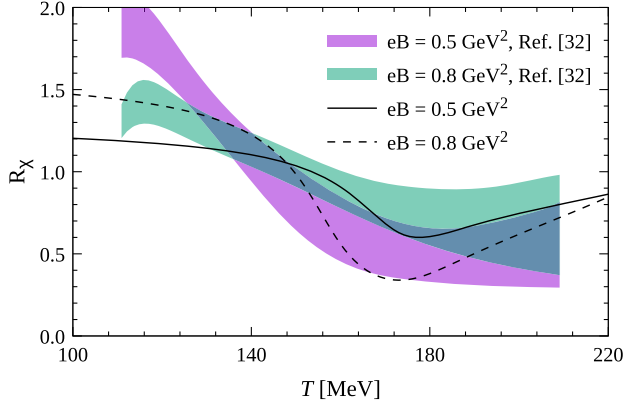


FIG. 5.  $\chi_t(B, T)/\chi_t(0, T)$  as a function of  $T$  for the case  $G = G(B)$ . The shaded bands correspond to lattice QCD results from Ref. [32].

In Fig. 6, we go back to our results for  $\chi_t^{1/4}$  and  $\lambda_a$  as functions of the temperature, this time normalizing  $\lambda_a$  to the corresponding value at  $T = 0$  and taking the magnetic field values  $eB = 0$  and  $eB = 0.4 \text{ GeV}^2$ , in order to compare our results (black solid lines) with those obtained within the two-flavor NJL model studied in Ref. [30] (red dashed lines). As in Fig. 5, our results correspond to  $G = G(B)$ , given by Eq. (37). The values of the temperature have been normalized to the critical temperatures  $T_c(B)$ , which are somewhat different for both models. This is in part due to the fact that in Ref. [30], an explicit dependence on both  $B$  and  $T$  has been assumed for the coupling  $G$ . It is seen that for the two-flavor model, the peak of  $\lambda_a$  at  $T = T_c$  is slightly higher, while the fall of both  $\chi_t^{1/4}$  and  $\lambda_a$  for  $T > T_c$  is less pronounced than in the case of the three-flavor NJL model. Nonetheless, it could be said that the behavior

of  $\chi_t^{1/4}$  and  $\lambda_a$  is found to be qualitatively similar for both models.

### C. Finite chemical potential

We turn now to discuss our numerical results for systems at nonzero quark chemical potential  $\mu$ . For a better comprehension, we start by briefly reviewing the phase diagrams in the  $\mu$ - $T$  plane, shown in Fig. 7. As expected, for low temperatures, the system undergoes a first-order chiral restoration transition at given critical chemical potentials  $\mu_c(B, T)$ . In the figure, we show the corresponding transition lines (solid lines in the figure) for some representative values of the magnetic field. These first-order transition lines finish at some critical end points (CEPs), whose positions depend on the external magnetic field. For higher values of the temperature, the transitions turn into smooth crossovers (dashed lines in the figure), as discussed for the systems at  $\mu = 0$ .

Left and right panels of Fig. 7 correspond to constant and  $B$ -dependent  $G$ , respectively. As stated, the assumption of a  $B$  dependence, such as the one in Eq. (37), leads to IMC, implying a significant change in the phase diagrams with respect to those obtained for the  $G = \text{constant}$  case. On the other hand, the behavior of the CEP with the magnetic field is known to be strongly model-dependent. It is seen that our results for the case  $G = G(B)$  are found to be qualitatively similar to those obtained in Ref. [57], where a three-flavor Polyakov-NJL model with a  $B$ -dependent coupling is studied; however, the behavior of the CEP is shown to be different from the one found in Ref. [58], where a nonlocal NJL-like model is considered (notice that in this type of model, IMC is naturally obtained [59,60]).

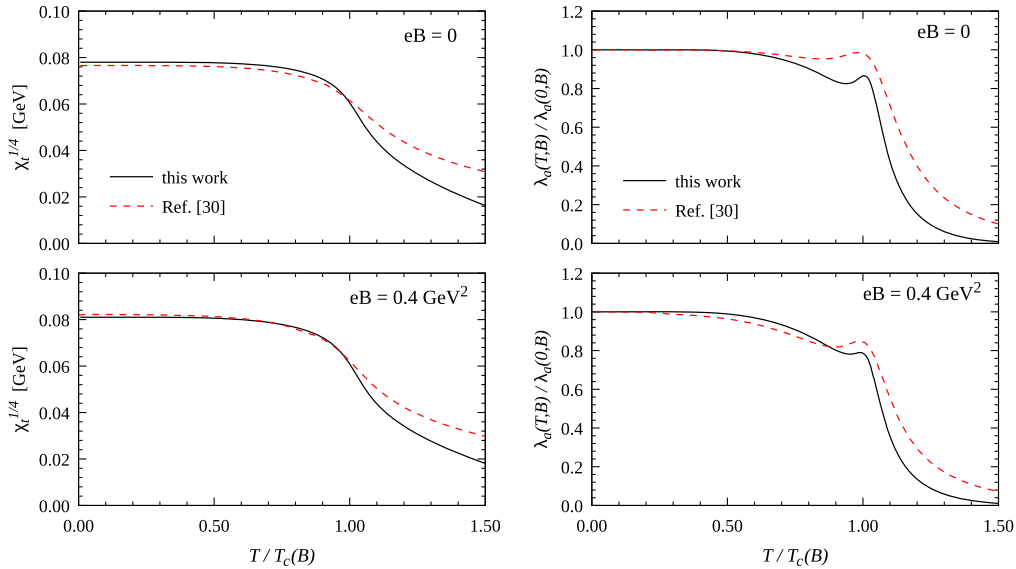


FIG. 6.  $\chi_t^{1/4}(B, T)$  (left) and  $\lambda_a(T, B)/\lambda_a(0, B)$  (right) as functions of  $T$  at  $\mu = 0$  for the case of  $G = G(B)$ . Our results (black solid lines) are compared with those obtained within a two-flavor NJL model in Ref. [30] (red dashed lines).

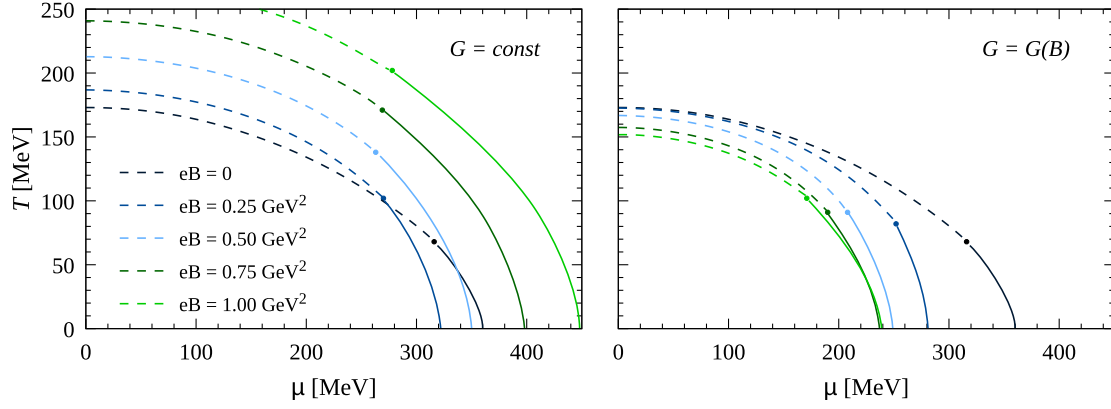


FIG. 7.  $\mu$ - $T$  phase diagrams for several values of the magnetic field. Solid (dashed) lines correspond to first-order (crossover) transitions, while critical end points are indicated by the fat dots. Left and right panels correspond to  $G = \text{constant}$  and  $G = G(B)$ , respectively.

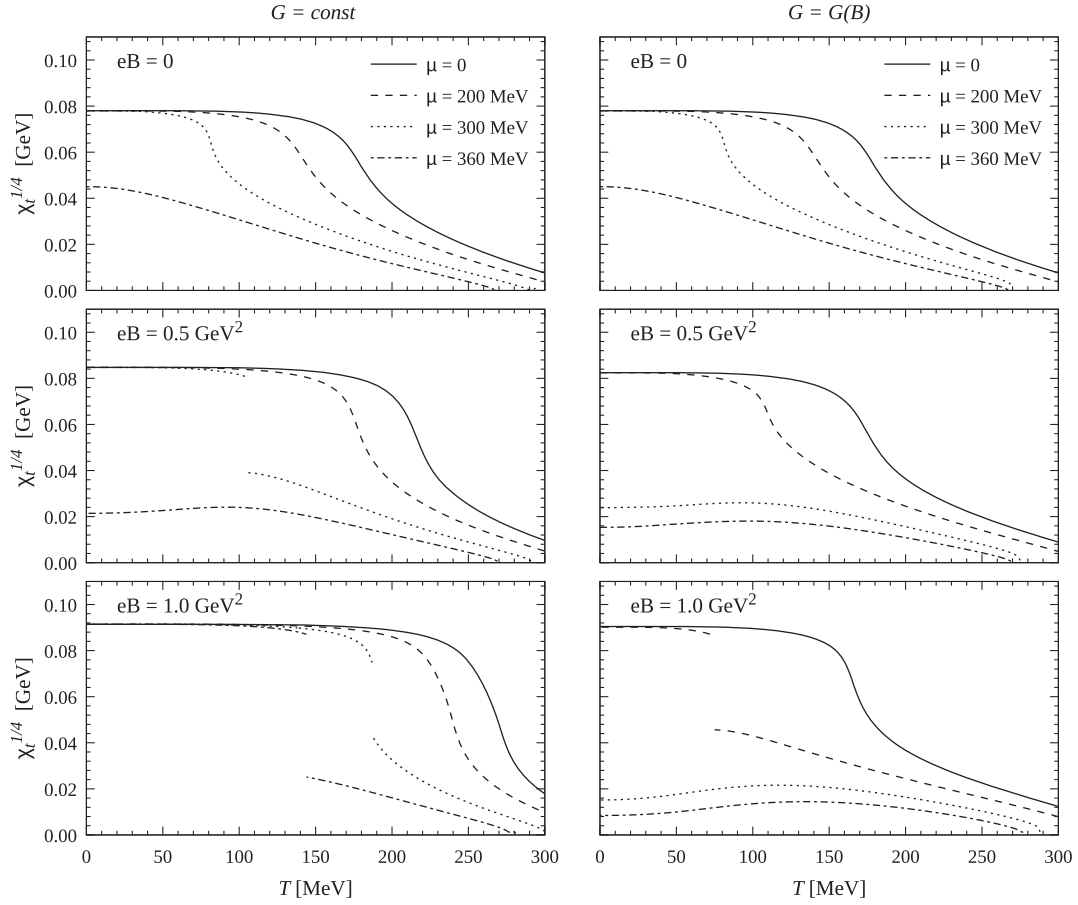


FIG. 8.  $\chi_t^{1/4}$  as a function of  $T$  for various values of the quark chemical potential and the magnetic field. Left and right panels correspond to  $G = \text{constant}$  and  $G = G(B)$ , respectively.

In Fig. 8, we show the behavior of  $\chi_t^{1/4}$  as a function of the temperature, taking some representative values of the chemical potential and the magnetic field. The curves clearly show the first-order and crossover transitions, both for the cases of  $G = \text{constant}$  (left panels) and  $G = G(B)$

(right panels). We have also verified that for nonzero  $\mu$ , the expressions in Eqs. (33) and (34) still approximate with good accuracy ( $\lesssim 1\%$ ) the exact result in Eq. (32), for temperatures that lie below the chiral transition. Then, in Fig. 9, we show the behavior of the axion self-coupling  $\lambda_a$

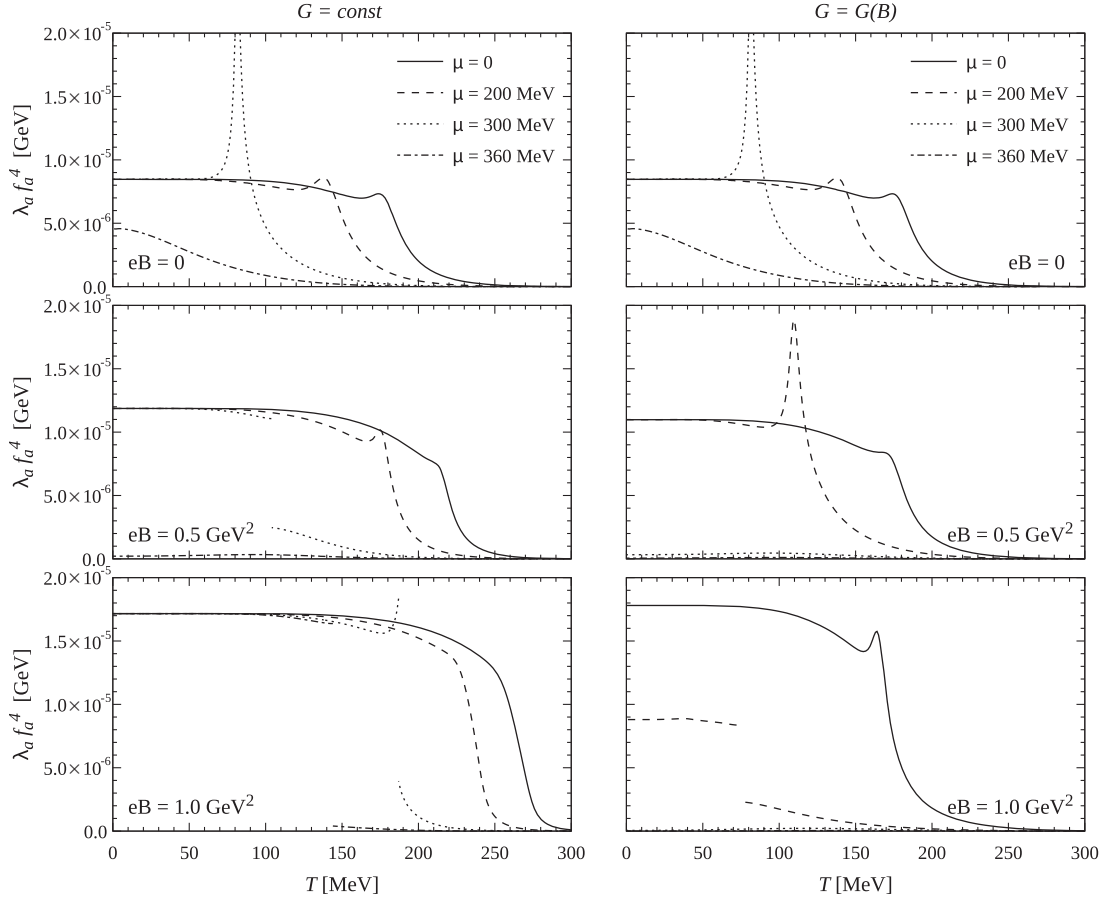


FIG. 9.  $\lambda_a f_a^4$  as a function of  $T$  for various values of the quark chemical potential and the magnetic field. Left and right panels correspond to  $G = \text{constant}$  and  $G = G(B)$ , respectively.

(times the dimensionful scale  $f_a^4$ ) for the same values of  $\mu$  and  $eB$ . It is seen that the peak in  $\lambda_a$ —which at  $\mu = 0$  was found to occur at the pseudocritical temperature—goes to infinity when the transition reaches the CEP, and turns into a first-order transition jump beyond the CEP. This feature has also been observed (for the  $B = 0$  case) in Ref. [21]. As mentioned in Ref. [20], there is no evident physical reason from which one can infer the presence of this peak—in that reference, it is argued that it could just arise as a consequence of working at the mean field level. In any case, our numerical results show that at the transition, the coupling  $\lambda_a$  behaves like the derivative of an order parameter; hence, it seems that within our approximations, the position of the peak could be used to define the pseudocritical transition temperature related to the restoration of the  $U(1)_A$  symmetry.

To conclude this section, we discuss the numerical results obtained for zero temperature and finite quark chemical potential. In Fig. 10, we show the behavior of the critical chemical potential  $\mu_c(B, 0)$  as a function of the magnetic field, both for constant and  $B$ -dependent couplings. The values are normalized to  $\mu_c(0, 0)$ . It is interesting to notice that for  $B \lesssim 0.3 \text{ GeV}^2$ , the models show again

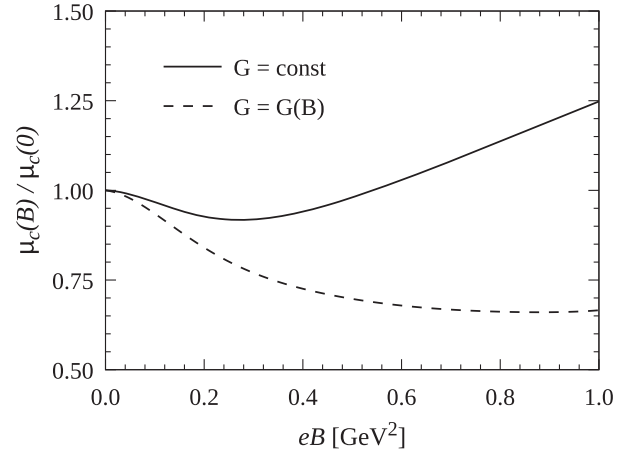


FIG. 10. Critical chemical potentials as functions of  $eB$  for zero temperature. Values are normalized to  $\mu_c(B = 0) = 359 \text{ MeV}$ . Solid and dashed lines correspond to  $G = \text{constant}$  and  $G = G(B)$ , respectively.

an IMC-like effect, i.e., a decrease of the critical chemical potential for increasing values of the magnetic field. This effect has been observed in various effective approaches to

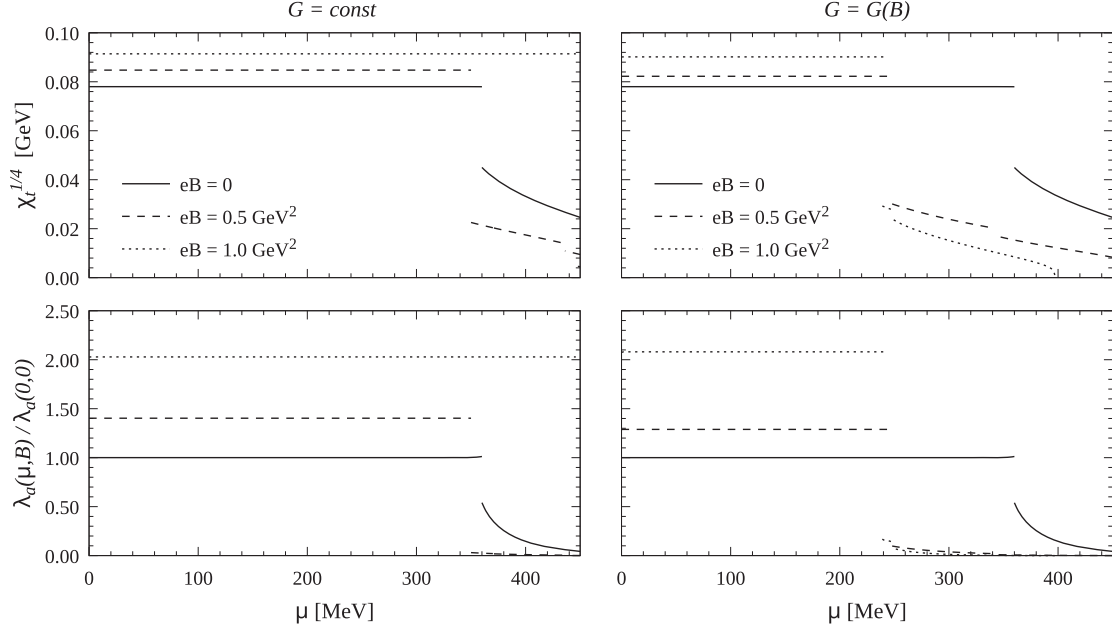


FIG. 11. Values of  $\chi_t^{1/4}$  and  $\lambda_a(\mu, B)/\lambda_a(0, 0)$  as functions of  $\mu$  for some representative values of the magnetic field. Left and right panels correspond to  $G = \text{constant}$  and  $G = G(B)$ , respectively.

low-energy QCD, including local and nonlocal NJL-like models [42,61–64]. For  $G = G(B)$ , it is seen that the IMC extends to larger values of the magnetic field, while for constant  $G$  the values of  $\mu_c$  reach a minimum and then get increased. This growth is consistent with the results in Ref. [63], where a constant value of  $G$  is assumed, while the persistent IMC behavior is similar to the one obtained in nonlocal NJL models [64], where nonlocality leads to an effective dependence of the couplings on the magnetic field [60].

In Fig. 11, we show the behavior of  $\chi_t^{1/4}$  and  $\lambda_a/\lambda_a(\mu = 0, B = 0)$  as functions of the chemical potential for three representative values of  $eB$ . Left and right panels correspond to constant and  $B$ -dependent couplings, respectively. The first-order chiral transitions can be clearly observed. Moreover, it can be seen that beyond these transitions, there is a second discontinuity, which corresponds to the partial chiral symmetry restoration related to the  $s$ -quark-antiquark condensate. Finally, in Fig. 12, we show the behavior of  $\chi_t^{1/4}$  and  $\lambda_a/\lambda_a(\mu = 0, B = 0)$  as functions of the magnetic field for some selected values of  $\mu$ . Here, we use a logarithmic scale, in order to focus on the region of low  $eB$ , and we just include the results for  $G = G(B)$  (the curves for  $G = \text{constant}$  are similar for values of  $eB$  up to about  $0.3 \text{ GeV}^2$ ). As one can see from Fig. 10, for low values of  $\mu$  the system lies in the chiral symmetry broken phase for all considered values of  $eB$ . Then, for  $\mu \gtrsim 230 \text{ MeV}$ , a first-order transition is found at some intermediate value of  $eB$ , while for values of  $\mu$  beyond  $\mu_c(0, 0) = 359 \text{ MeV}$  the system lies in the partially restored chiral symmetry phase.

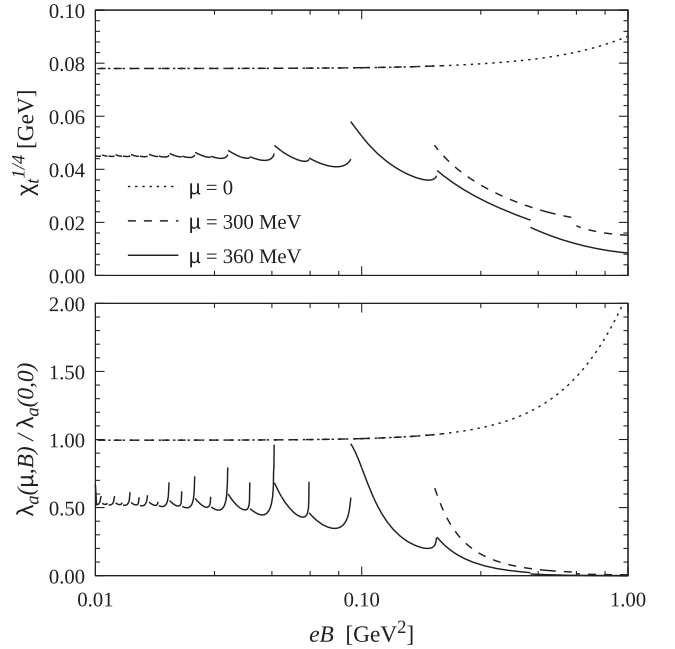


FIG. 12. Values of  $\chi_t^{1/4}$  and  $\lambda_a(\mu, B)/\lambda_a(0, 0)$  as functions of  $eB$  for some representative values of the quark chemical potential. The curves correspond to the case  $G = G(B)$ .

Typically, in this region, one finds for  $T = 0$  a series of magnetic oscillations related to the van Alphen–de Haas effect [37]. In fact, as shown in the figure, one finds a sequence of first-order transitions that correspond to the values of  $\mu$  that satisfy the relation  $\mu^2 = 2kB_f + \bar{M}_f^2$

( $f = u, d$ ) for integer  $k$ . The value of  $\chi_t^{1/4}$  is found to be relatively large for  $\mu$  right above  $\mu_c$  at low values of the magnetic field, and becomes significantly reduced when  $eB$  is increased up to  $\sim 1 \text{ GeV}^2$ .

#### IV. SUMMARY AND CONCLUSIONS

In the present work, we have analyzed the topological susceptibility and the axion properties in the presence of a strong magnetic field, considering a three-flavor NJL model that includes strong  $CP$  violation through a 't Hooft-like flavor mixing term. The behavior of the relevant quantities for systems at finite temperature and quark chemical potential have been studied.

As is well known, when the scalar/pseudoscalar coupling  $G$  is kept constant (i.e., when it does not depend on the magnetic field), local NJL models are not able to reproduce the inverse magnetic catalysis effect at finite temperature. Therefore, we have considered both the case of a constant  $G$  and the one in which one assumes a  $B$ -dependent coupling  $G = G(B)$ , chosen in such a way that the model is able to adequately reproduce the  $B$  dependence of the critical chiral transition temperatures obtained in lattice QCD.

We have shown that within these three-flavor NJL models, the topological susceptibility has a rather simple expression [see Eq. (32)] in terms of the quark condensates, the current quark masses, and the strength of the flavor mixing term. In addition, we have shown that close to the chiral limit, this expression reduces to the one obtained in other approaches to nonperturbative QCD, such as chiral perturbation theory [29,45] and the linear sigma model [46].

At  $T = \mu = 0$ , using standard values of model parameters, we obtain, for the vanishing external magnetic field,  $\chi_t = 78 \text{ MeV}$  and  $\lambda_a = 0.85 \times 10^{-5} \text{ GeV}^4/f_a^4$ , in reasonable agreement with values obtained from LQCD and/or ChPT [65]. For the nonzero magnetic field, in agreement with previous analyses, we find that the topological susceptibility gets increased with  $B$ . Clearly, this can be understood by noticing that, according to the previously mentioned theoretical expressions,  $\chi_t$  is approximately proportional to the quark condensates, which exhibit the well-known magnetic catalysis effect. Moreover, we find that the axion self-coupling  $\lambda_a$  also increases with the magnetic field.

For the case of both nonzero temperature and magnetic field, we find that, as expected,  $\chi_t$  and  $\lambda_a$  remain approximately constant as functions of  $T$ , up to the critical temperatures  $T_c(B)$ . Beyond these values, we find for both quantities a sudden drop, signaling the restoration of the  $U(1)_A$  symmetry in the light quark sector. We also note that the curves for  $\lambda_a$  tend to show a peak located at  $T = T_c$ . When comparing our results with those of the  $SU(2)$  NJL

model analyzed in Ref. [30], it is seen that for the two-flavor model, the peak of  $\lambda_a$  at  $T = T_c$  is slightly higher, while the fall of both  $\chi_t^{1/4}$  and  $\lambda_a$  observed for  $T > T_c$  is less pronounced than in the case of the three-flavor model. In any case, it could be said that the behavior of  $\chi_t^{1/4}$  and  $\lambda_a$  is found to be qualitatively similar for both models. Regarding the comparison with finite temperature LQCD, our predictions for  $R_\chi = \chi_t(B, T)/\chi_t(0, T)$  in the case of the  $B$ -dependent coupling  $G(B)$  show qualitative agreement with those obtained from LQCD calculations.

As stated, we have completed our analysis by considering systems at nonzero quark chemical potential. Curves showing the behavior of  $\chi_t$  and  $\lambda_a$  as functions of the temperature are given for various values of the chemical potential, showing both crossover and first-order transitions. It is found that the approximate expressions for  $\chi_t$  in Eqs. (33) and (34) work very well (within  $\simeq 2\%$ ) in the chirally broken phase (i.e., at low temperatures and/or chemical potentials), whereas they show some deviation in the restored phase. In the case of crossover transitions, it is seen that  $\lambda_a$  behaves like the derivative of an order parameter; thus, the position of the corresponding peak can be used to define the pseudocritical transition temperature associated with the restoration of  $U(1)_A$  symmetry. At zero temperature and finite  $\mu$ , it is seen that for  $G = G(B)$ , the critical chemical potentials exhibit inverse magnetic catalysis, showing a similar behavior as the one observed in nonlocal NJL-like models. In the chirally restored phase, for  $T = 0$  and low magnetic fields, we observe a pattern of magnetic oscillations in the values of both  $\lambda_a$  and  $\chi_t$ , related to the well-known van Alphen–de Haas effect.

In general, it is seen that the case in which  $G = G(B)$ , which (by construction) exhibits inverse magnetic catalysis at finite temperature, provides the best agreement with results from LQCD at zero chemical potential and yields a phase diagram that is consistent with the expected phenomenology at finite chemical potential. We find that the behavior of  $\lambda_a(T, \mu, B)$  and  $\chi_t(T, \mu, B)$  is predominantly determined by the light quark condensates, i.e., by the chiral  $SU(2)$  symmetry restoration, and shows reasonable agreement with other effective models, including approximate results from chiral perturbation theory.

#### ACKNOWLEDGMENTS

This work has been supported in part by Consejo Nacional de Investigaciones Científicas y Técnicas and Agencia Nacional de Promoción Científica y Tecnológica (Argentina), under Grants No. PIP2022-GI-11220210100150CO, No. PICT20-01847, and No. PICT22-03-00799, and by the National University of La Plata (Argentina), Project No. X960.

### DATA AVAILABILITY

The data that support the findings of this article are not publicly available upon publication because it is not technically feasible and/or the cost of preparing, depositing, and hosting the data would be prohibitive within the terms of this research project. The data are available from the authors upon reasonable request.

### APPENDIX

In this appendix, we sketch the steps followed to obtain our main analytical results, given by Eqs. (30) and (32). From Eq. (5), together with the conditions in Eqs. (28) and (29), one has

$$\frac{d\Omega}{d\theta} = \frac{\partial\Omega}{\partial\theta} = -\frac{K}{24} \sum_{ijk} |\epsilon_{ijk}| [\sin\theta (\bar{s}_i \bar{s}_j \bar{s}_k - 3\bar{s}_i \bar{p}_j \bar{p}_k) + \cos\theta (\bar{p}_i \bar{p}_j \bar{p}_k - 3\bar{p}_i \bar{s}_j \bar{s}_k)]. \quad (\text{A1})$$

Using Eqs. (7) and (8), and noting that  $\bar{s}_f M_{pf} = \bar{p}_f M_{sf}$  [see Eq. (13)], one gets

$$\frac{d\Omega}{d\theta} = -\frac{1}{6} \sum_f m_f \bar{p}_f, \quad (\text{A2})$$

where  $m_f$  are the current quark masses.

Now it can be shown that the terms in the above sum over flavors are equal to each other. Indeed, from Eqs. (7) and (8), one has

$$\begin{aligned} m_i \bar{p}_i &= \frac{K}{4} \sum_{jk} |\epsilon_{ijk}| [\bar{p}_i \bar{p}_j \bar{p}_k \cos\theta + \bar{s}_i \bar{s}_j \bar{s}_k \sin\theta \\ &\quad - (\bar{p}_i \bar{s}_j \bar{s}_k + 2\bar{s}_i \bar{p}_j \bar{s}_k) \cos\theta - (\bar{s}_i \bar{p}_j \bar{p}_k + 2\bar{p}_i \bar{s}_j \bar{p}_k) \sin\theta] \\ &= \frac{K}{12} \sum_{ljk} |\epsilon_{ljk}| [\bar{p}_l (\bar{p}_j \bar{p}_k - 3\bar{s}_j \bar{s}_k) \cos\theta \\ &\quad + \bar{s}_l (\bar{s}_j \bar{s}_k - 3\bar{p}_j \bar{p}_k) \sin\theta], \end{aligned} \quad (\text{A3})$$

where the last expression does not depend on  $i$ . To derive the second equality, we have used the property

$$\sum_{jk} |\epsilon_{ijk}| (a_i b_j b_k + 2b_i a_j b_k) = \sum_{ljk} |\epsilon_{ljk}| a_l b_j b_k. \quad (\text{A4})$$

Since  $m_u \bar{p}_u = m_d \bar{p}_d = m_s \bar{p}_s$ , Eq. (A2) can be written as

$$\frac{d\Omega}{d\theta} = -\frac{1}{2} m_f \bar{p}_f, \quad (\text{A5})$$

where  $f$  can be either  $u$ ,  $d$ , or  $s$ .

We turn now to evaluate the second derivative in Eqs. (27) and (31). According to the above expression for  $d\Omega/d\theta$ , we need to determine  $d\bar{p}_f/d\theta$ . We have

$$\frac{d\bar{p}_f}{d\theta} = \frac{\partial\bar{p}_f}{\partial\bar{\sigma}_f} \frac{\partial\bar{\sigma}_f}{\partial\theta} + \frac{\partial\bar{p}_f}{\partial\bar{\pi}_f} \frac{\partial\bar{\pi}_f}{\partial\theta}. \quad (\text{A6})$$

The expressions for  $\partial\bar{p}_f/\partial\bar{\sigma}_f$  and  $\partial\bar{p}_f/\partial\bar{\pi}_f$  can be readily obtained from Eq. (13) and the subsequent expressions of the functions  $I_{1f}$  for zero and nonzero temperature. On the other hand, the partial derivatives of  $\bar{\sigma}_f$  and  $\bar{\pi}_f$  with respect to  $\theta$  can be calculated by solving the coupled equations

$$\begin{aligned} \frac{\partial\bar{\sigma}_i}{\partial\theta} + \sum_{\phi=\bar{\sigma},\bar{\pi}} \left[ 2G \frac{\partial\bar{\sigma}_i}{\partial\phi_i} \frac{\partial\phi_i}{\partial\theta} - \frac{K}{2} \sum_{jk} |\epsilon_{ijk}| \right. \\ \left. \times \left( \frac{\partial\bar{s}_j}{\partial\phi_j} \bar{s}_{\theta,k} - \frac{\partial\bar{p}_j}{\partial\phi_j} \bar{p}_{\theta,k} \right) \frac{\partial\phi_j}{\partial\theta} \right] = -\bar{\pi}_i - 2G\bar{p}_i, \end{aligned} \quad (\text{A7})$$

$$\begin{aligned} \frac{\partial\bar{\pi}_i}{\partial\theta} + \sum_{\phi=\bar{\sigma},\bar{\pi}} \left[ 2G \frac{\partial\bar{p}_i}{\partial\phi_i} \frac{\partial\phi_i}{\partial\theta} + \frac{K}{2} \sum_{jk} |\epsilon_{ijk}| \right. \\ \left. \times \left( \frac{\partial\bar{s}_j}{\partial\phi_j} \bar{p}_{\theta,k} + \frac{\partial\bar{p}_j}{\partial\phi_j} \bar{s}_{\theta,k} \right) \frac{\partial\phi_j}{\partial\theta} \right] = \bar{\sigma}_i + 2G\bar{s}_i, \end{aligned} \quad (\text{A8})$$

where we have introduced the shorthand notation

$$\bar{s}_{\theta,k} = \bar{s}_k \cos\theta + \bar{p}_k \sin\theta, \quad \bar{p}_{\theta,k} = \bar{p}_k \cos\theta - \bar{s}_k \sin\theta. \quad (\text{A9})$$

The calculation of the topological susceptibility  $\chi_t$  requires the evaluation of  $d^2\Omega/d\theta^2$  in the limit  $\theta=0$ , where the equations get simplified. One has, in this case,

$$\bar{p}_f = 0, \quad \bar{\pi}_f = 0, \quad \frac{\partial\bar{p}_f}{\partial\bar{\sigma}_f} = 0, \quad \frac{\partial\bar{p}_f}{\partial\bar{\pi}_f} = \frac{\bar{s}_f}{M_{sf}}. \quad (\text{A10})$$

Moreover, from Eq. (A8), we get

$$\frac{\partial\bar{\pi}_i}{\partial\theta} \left[ 1 + \frac{2G\bar{s}_i}{M_{si}} + \frac{Km_i\bar{s}_i}{2M_{si}} \sum_{jk} |\epsilon_{ijk}| \frac{\partial\bar{s}_k}{m_j} \right] = \bar{\sigma}_i + 2G\bar{s}_i, \quad (\text{A11})$$

where we have made use of the fact that the product

$$m_f \frac{d\bar{p}_f}{d\theta} = \frac{m_f \bar{s}_f}{M_{sf}} \frac{\partial\bar{\pi}_f}{\partial\theta} \quad (\text{A12})$$

does not depend on the flavor  $f$ . From Eqs. (7) and (A11), using the property in Eq. (A4) and the relation

$$\bar{s}_i \sum_{jk} |\epsilon_{ijk}| \bar{s}_j \bar{s}_k = 2\bar{s}_u \bar{s}_d \bar{s}_s, \quad (\text{A13})$$

one arrives at the result in Eq. (32), namely,

$$\chi_t = \frac{d^2\Omega}{d\theta^2} \Big|_{\theta=0} = -\frac{1}{2} \left[ \frac{2}{K\bar{s}_u\bar{s}_d\bar{s}_s} + \sum_k \frac{1}{m_k\bar{s}_k} \right]^{-1}. \quad (\text{A14})$$

- 
- [1] A. A. Belavin, A. M. Polyakov, A. S. Schwartz, and Y. S. Tyupkin, *Phys. Lett.* **59B**, 85 (1975).
- [2] C. G. Callan, Jr., R. F. Dashen, and D. J. Gross, *Phys. Lett.* **63B**, 334 (1976).
- [3] R. D. Peccei and H. R. Quinn, *Phys. Rev. Lett.* **38**, 1440 (1977).
- [4] R. D. Peccei, *Lect. Notes Phys.* **741**, 3 (2008).
- [5] L. Di Luzio, M. Giannotti, E. Nardi, and L. Visinelli, *Phys. Rep.* **870**, 1 (2020).
- [6] S. Navas *et al.* (Particle Data Group), *Phys. Rev. D* **110**, 030001 (2024).
- [7] J. Preskill, M. B. Wise, and F. Wilczek, *Phys. Lett.* **120B**, 127 (1983).
- [8] L. F. Abbott and P. Sikivie, *Phys. Lett.* **120B**, 133 (1983).
- [9] M. Dine and W. Fischler, *Phys. Lett.* **120B**, 137 (1983).
- [10] A. Caputo and G. Raffelt, *Proc. Sci. COSMICWISPerS* (2024) 041 [arXiv:2401.13728].
- [11] A. Sedrakian, *Phys. Rev. D* **93**, 065044 (2016).
- [12] S. Borsanyi, Z. Fodor, J. Guenther, K. H. Kampert, S. D. Katz, T. Kawanai, T. G. Kovacs, S. W. Mages, A. Pasztor, F. Pittler *et al.*, *Nature (London)* **539**, 69 (2016).
- [13] P. Petreczky, H. P. Schadler, and S. Sharma, *Phys. Lett. B* **762**, 498 (2016).
- [14] Y. Taniguchi, K. Kanaya, H. Suzuki, and T. Umeda, *Phys. Rev. D* **95**, 054502 (2017).
- [15] K. Fukushima, K. Ohnishi, and K. Ohta, *Phys. Rev. C* **63**, 045203 (2001).
- [16] P. Costa, M. C. Ruivo, C. A. de Sousa, H. Hansen, and W. M. Alberico, *Phys. Rev. D* **79**, 116003 (2009).
- [17] G. A. Contrera, D. G. Dumm, and N. N. Scoccola, *Phys. Rev. D* **81**, 054005 (2010).
- [18] Z. Y. Lu and M. Ruggieri, *Phys. Rev. D* **100**, 014013 (2019).
- [19] B. S. Lopes, R. L. S. Farias, V. Dexheimer, A. Bandyopadhyay, and R. O. Ramos, *Phys. Rev. D* **106**, L121301 (2022).
- [20] A. Abhishek, A. Das, H. Mishra, and R. K. Mohapatra, *Phys. Rev. D* **103**, 074003 (2021).
- [21] B. Zhang, D. E. A. Castillo, A. G. Grunfeld, and M. Ruggieri, *Phys. Rev. D* **108**, 054010 (2023).
- [22] H. F. Gong, Q. Lu, Z. Y. Lu, L. M. Liu, X. Chen, and S. P. Wang, *Eur. Phys. J. C* **84**, 1222 (2024).
- [23] F. Murgana, D. E. A. Castillo, A. G. Grunfeld, and M. Ruggieri, *Phys. Rev. D* **110**, 014042 (2024).
- [24] K. Fukushima, D. E. Kharzeev, and H. J. Warringa, *Phys. Rev. D* **78**, 074033 (2008).
- [25] D. E. Kharzeev, J. Liao, and P. Tribedy, *Int. J. Mod. Phys. E* **33**, 2430007 (2024).
- [26] M. Asakawa, A. Majumder, and B. Muller, *Phys. Rev. C* **81**, 064912 (2010).
- [27] P. Adhikari, *Phys. Lett. B* **825**, 136826 (2022).
- [28] P. Adhikari, *Nucl. Phys.* **B974**, 115627 (2022).
- [29] P. Adhikari, *Nucl. Phys.* **B982**, 115853 (2022).
- [30] A. Bandyopadhyay, R. L. S. Farias, B. S. Lopes, and R. O. Ramos, *Phys. Rev. D* **100**, 076021 (2019).
- [31] M. S. Ali, C. A. Islam, and R. Sharma, *Phys. Rev. D* **104**, 114026 (2021).
- [32] B. B. Brandt, G. Endrődi, J. J. H. Hernández, and G. Markó, *J. High Energy Phys.* **12** (2025) 228.
- [33] B. Chatterjee, H. Mishra, and A. Mishra, *Phys. Rev. D* **91**, 034031 (2015).
- [34] J. K. Boomsma and D. Boer, *Phys. Rev. D* **80**, 034019 (2009).
- [35] V. A. Miransky and I. A. Shovkovy, *Phys. Rep.* **576**, 1 (2015).
- [36] J. O. Andersen, W. R. Naylor, and A. Tranberg, *Rev. Mod. Phys.* **88**, 025001 (2016).
- [37] D. Ebert, K. G. Klimenko, M. A. Vdovichenko, and A. S. Vshivtsev, *Phys. Rev. D* **61**, 025005 (2000).
- [38] M. A. Vdovichenko, A. S. Vshivtsev, and K. G. Klimenko, *Phys. At. Nucl.* **63**, 470 (2000).
- [39] D. Ebert and K. G. Klimenko, *Nucl. Phys.* **A728**, 203 (2003).
- [40] D. P. Menezes, M. Benghi Pinto, S. S. Avancini, A. Perez Martinez, and C. Providencia, *Phys. Rev. C* **79**, 035807 (2009).
- [41] D. P. Menezes, M. Benghi Pinto, S. S. Avancini, and C. Providencia, *Phys. Rev. C* **80**, 065805 (2009).
- [42] P. G. Allen, A. G. Grunfeld, and N. N. Scoccola, *Phys. Rev. D* **92**, 074041 (2015).
- [43] S. S. Avancini, W. R. Tavares, and M. B. Pinto, *Phys. Rev. D* **93**, 014010 (2016).
- [44] M. Coppola, D. Gomez Dumm, and N. N. Scoccola, *Phys. Lett. B* **782**, 155 (2018).
- [45] Y. Y. Mao and T.-W. Chiu (TWQCD Collaboration), *Phys. Rev. D* **80**, 034502 (2009).
- [46] M. Kawaguchi, S. Matsuzaki, and A. Tomiya, *Phys. Rev. D* **103**, 054034 (2021).
- [47] H. Leutwyler and A. V. Smilga, *Phys. Rev. D* **46**, 5607 (1992).
- [48] P. Rehberg, S. P. Klevansky, and J. Hufner, *Phys. Rev. C* **53**, 410 (1996).
- [49] M. Coppola, W. R. Tavares, S. S. Avancini, J. C. Sodr , and N. N. Scoccola, *Phys. Rev. D* **110**, 114036 (2024).

- [50] M. Ferreira, P. Costa, O. Lourenço, T. Frederico, and C. Providência, [Phys. Rev. D \*\*89\*\*, 116011 \(2014\)](#).
- [51] R. L. S. Farias, K. P. Gomes, G. I. Krein, and M. B. Pinto, [Phys. Rev. C \*\*90\*\*, 025203 \(2014\)](#).
- [52] R. L. S. Farias, V. S. Timoteo, S. S. Avancini, M. B. Pinto, and G. Krein, [Eur. Phys. J. A \*\*53\*\*, 101 \(2017\)](#).
- [53] G. S. Bali, F. Bruckmann, G. Endrodi, Z. Fodor, S. D. Katz, S. Krieg, A. Schafer, and K. K. Szabo, [J. High Energy Phys. \*\*02\*\* \(2012\) 044](#).
- [54] A. Bazavov *et al.* (HotQCD Collaboration), [Phys. Lett. B \*\*795\*\*, 15 \(2019\)](#).
- [55] M. Gorghetto and G. Villadoro, [J. High Energy Phys. \*\*03\*\* \(2019\) 033](#).
- [56] G. Grilli di Cortona, E. Hardy, J. Pardo Vega, and G. Villadoro, [J. High Energy Phys. \*\*01\*\* \(2016\) 034](#).
- [57] P. Costa, M. Ferreira, D. P. Menezes, J. Moreira, and C. Providência, [Phys. Rev. D \*\*92\*\*, 036012 \(2015\)](#).
- [58] J. P. Carlomagno, S. A. Ferraris, D. Gomez Dumm, and A. G. Grunfeld, [Phys. Rev. D \*\*108\*\*, 056029 \(2023\)](#).
- [59] V. P. Pagura, D. Gomez Dumm, S. Noguera, and N. N. Scoccola, [Phys. Rev. D \*\*95\*\*, 034013 \(2017\)](#).
- [60] D. Gómez Dumm, M. F. Izzo Villafañe, S. Noguera, V. P. Pagura, and N. N. Scoccola, [Phys. Rev. D \*\*96\*\*, 114012 \(2017\)](#).
- [61] F. Preis, A. Rebhan, and A. Schmitt, [J. High Energy Phys. \*\*03\*\* \(2011\) 033](#).
- [62] F. Preis, A. Rebhan, and A. Schmitt, [Lect. Notes Phys. \*\*871\*\*, 51 \(2013\)](#).
- [63] P. G. Allen and N. N. Scoccola, [Phys. Rev. D \*\*88\*\*, 094005 \(2013\)](#).
- [64] S. A. Ferraris, D. G. Dumm, A. G. Grunfeld, and N. N. Scoccola, [Eur. Phys. J. A \*\*57\*\*, 141 \(2021\)](#).
- [65] Z. Y. Lu, M. L. Du, F. K. Guo, U. G. Meißner, and T. Vonk, [J. High Energy Phys. \*\*05\*\* \(2020\) 001](#).